CrossMark

Investigating surface properties of cryogenically treated titanium alloys in powder mixed electric discharge machining

Sanjeev Kumar[1] · Rupinder Singh[2] · Ajay Batish[3] · T. P. Singh[4] · Rajdeep Singh[1]

Abstract Although electrical discharge machining is a metal removal process in form of debris, efforts have been made in this article to make use of this process as a surface treatment method. Effect of different process parameters and mechanism of material deposition also studied under this study. Powder mixed electric discharge machining (PMEDM) process has been used which helps in improving the surface properties. In this study, changes in surface properties of cryogenically treated titanium alloy after PMEDM process were investigated. Experimental results showed significant improvement in micro-hardness by 94.85 %. Various studies, like scanning electron microscopy (SEM), energy-dispersive X-ray spectroscopy (EDX), and X-ray diffraction (XRD) were carried out to study the characteristics of the machined surface. After scanning the machined surface through XRD and EDX, the transfer of various elements from electrode material and powder mixed dielectric and their chemical compounds were observed. After screening the results, peak current was observed as the highly influential parameter that affected the micro-hardness as well as surface quality of the machined surface.

Technical Editor: Márcio Bacci da Silva.

✉ Sanjeev Kumar
    sanjeevsharma_69@yahoo.co.in

1   Department of Mechanical Engineering, Chandigarh Engineering College, Landran, Chandigarh, Punjab, India

2   Department of Production Engineering, GNDEC, Ludhiana, Punjab 141006, India

3   Department of Mechanical Engineering, Thapar University, Patiala, Punjab 141004, India

4   Symbiosis Institute of Technology, Pune, Maharashtra 411016, India

1 Introduction

Titanium (Ti) alloys find usage in different industries, namely automobile, chemical, manufacturing, and medical, due to its excellent properties. Titanium is alloyed with aluminum (Al), vanadium (V), tin (Sn), zirconium (Zr), manganese (Mn), molybdenum (Mo), and other metals to increase its strength, so that it can withstand at high temperatures [1]. Thus, a most widely used non-conventional thermo-electric machining process "Electric Discharge Machining" (EDM) has been selected for machining of titanium and its alloys irrespective of its hardness and high strength during this study. In EDM, the material is removed due to repeated electric sparks in dielectric fluid, resulting in generation of high temperature in the range of 8000–12,000 °C [2].

A lot of research works were reported by the researchers on different machining aspects in conventional EDM, which have some limitation like low material removal rate, higher tool wear, rough surface texture, and low surface hardness with inferior surface properties. To overcome these limitations of ordinary EDM process, hybrid EDM has been tried out. In this study, to improve the surface properties and machining efficiency, powder particles were mixed with dielectric fluid during EDM process, known as PMEDM. During this process, some of the metal elements were transferred and deposited on the machined surface either in free form or compound form under the influence of suitable machining conditions. This issue leads to changes in chemical composition of the

machined surface, thus, improves the surface properties in terms of surface hardness or microstructure/metallurgical. In this article, extensive literature based on material transfer and surface modification has been discussed in brief. Lin et al. successfully used a combination of EDM with USM process and concluded that the thickness of the recast layer decreased when distilled water was used as dielectric [3]. Yan et al. applied magnetic abrasive finishing process with EDM to improve the surface properties by removing the recast layer and micro-cracks [4]. Yan et al. explored the effect of urea mixed dielectric on machining characteristics of pure titanium. Due to formation of hard layer of titanium-nitride (TiN), micro-hardness of the machined surface was increased resulting in producing good wear resistance surface [5]. Hascalik and Caydus explored the effect of different electrode materials on the surface quality of Ti–6Al–4V and observed hard compound of titanium-carbide ($Ti_{24}C_{15}$) with graphite electrode, resulting in higher surface hardness [6]. Pardhan et al. reported that low values of peak current and pulse-on-time give better surface properties than higher value of current and on-time while machining Ti–6Al–4V [7]. Kibria et al. studied the effect of boron-carbide (B_4C) powder with kerosene and deionized water dielectric fluid during EDM of Ti–6Al–4V [8]. Kao et al. studied the machining characteristics with the surface integrity of Ti–6Al–4V and noticed traces of TiC on specimen [2]. Lin and Lee analyzed the surface integrity through SEM to study the effects of magnetic force [9]. An experimental investigation was carried out by Jabbaripour et al. by varying current, pulse-on-time, and open circuit voltage, to explore their effects on surface topography and recast layer [10]. Chow et al. explored the effect of SiC and Al powder with kerosene oil during micro-slit machining of Ti–6Al–4V alloy [11]. Batish et al. attempted to improve the surface integrity of three different die steel materials using the graphite and aluminum powder [12]. Kumar et al. reported significant improvement in surface characteristics using Al and Si powder with dielectric [13, 14]. The significant improvement in hardness by 73 % with no micro-cracks was observed when manganese (Mn) powder was used [15]. Surface modification of Al workpiece highly increased from a base metal value of 150–1800 HV using powder metallurgy TiC/Cu green compact electrode with electric discharge coating (EDC) process [16]. Significant improvements for SKD11 and Ti–6Al–4V alloy were observed using Al and SiC powder mixed dielectric [17–19]. Kansal et al. used Si powder with different concentration and concluded that machining performance was improved [20]. Khan et al. investigated the effect of different process parameters and electrode material on surface finish and micro-structural properties of Ti–5Al–2.5Sn titanium alloys [26].

In the past, researchers also used cryogenic treatment and cold treatment to increase efficiency of conventional EDM process. A few studies were reported on using cryogenic treatment in the field of EDM. Abdulkareem et al. reduced the electrode wear ratio and surface roughness using cryogenically cooled copper electrode during EDM of Ti–6Al–4V [21]. Gill and Singh attempted to compare the accuracy of holes drilled in without cryogenically treated and deep cryogenically treated (DCT) Ti6246 titanium alloy in terms of surface roughness and over cut [22]. Srivastava and Pandey experimentally observed better surface integrity when machining was performed with ultrasonic-assisted cryogenically cooling electrode [23]. Jafferson and Hariharan compared the machining performance in terms of electrical resistivity, crystallite size, microhardness, and microscopic analysis of cryogenically treated and untreated micro electrode and observed significant improvement with cryogenically treated electrodes [24].

From the literature review, it was observed that a number of studies have been reported on the EDM of titanium alloys for process control and optimization of parameters. Surface modification of titanium alloys through material transfer mechanism is still at the experimental stage. Even, no study was conducted using cryogenic treatment (shallow and deep) on both workpiece and electrode simultaneously. Even, no study was performed using manganese (Mn) and tungsten (W) powder during machining of titanium alloys. Still, no study was conducted on TI–5Al–2.5Sn alloy with Cu–Cr electrode. The formation of various compounds on the machined surface due to material transfer either from powder mixed dielectric or electrode material and its effect on surface modification needs to be investigated through experiments. The surface modifications were measured in terms of change in surface hardness, i.e., before and after machining. L_{18} orthogonal array of Taguchi's fractional factorial design was used for design of experiments (DOE) consisting eight factors. The changes in surface properties after machining were analyzed through SEM, XRD, and EDX analyzer.

2 Experimental procedures

2.1 Experimental setup

The experiments were performed on CNC Die Sinking Electric Discharge Machine, Model S 645 C MAX with positive polarity of tool. A separate small metal container was used in place of main machine tank to avoid the wastage of dielectric. A motorized stirrer was fixed at the left corner of small tank for proper mixing and to avoid settling of powder particles. A suitable fixture was developed to hold the workpiece when placed inside this tank.

2.2 Materials

Three workpiece materials TITAN 15 ASTM Grade 2 (Ti 99.83 %), TITAN 21 ASTM Grade 6 (5.32 % Al, 2.76 % Sn, and 91.8 % Ti) and TITAN 31 ASTM Grade 5 (6.19 % Al, 4.04 % V, and 89.6 % Ti) were machined during this study. The tool materials (18 mm diameter) used were electrolytic copper (99.5 % Cu, 0.175 % Zn), copper–chromium (99.2 % Cu, 0.605 Cr), and copper–tungsten (29.27 % Cu, 68.1 % W). Ferrolac 3 M EDM oil was used as dielectric fluid. Manganese (325 Mesh, 44 microns) and tungsten (3-5 micron) powder of concentration 10 g/l and pure 99.5 % was used with dielectric oil to explore their effect on surface properties.

2.3 Cryogenic treatment

Cryogenic Processor (model; Primero EnServe, CP 220LH) with temperature range −184 to 150 °C having a size of 450 mm × 1200 mm × 450 mm was used for cryogenic treatment of workpiece and electrode materials. The workpiece and electrode were cryogenically treated at two different temperature conditions. For Shallow Cryogenic Treatment (SCT), the material was cooled to −110 °C and held for 6 h and then heated up to ambient temperature. For Deep Cryogenic Treatment (DCT), the material was cooled to −184 °C and held for 24 h and then heated to ambient temperature at the same rate. Thereafter, the only work material was tempered at 150 °C for 2 h for stress relieving. Cooling and heating rate of 1 °C/min was maintained during the entire cycle. Figure 1 shows the photographic view of cryogenic processor used for cryogenic treatment of work and tool materials.

Fig. 1 Photographic view of cryogenic processor

Table 1 Machining parameters

(A) Pulse-off-time (T_{off})	30, 45 μs
(B) Peak current (I_p)	06, 10, 14 A
(C) Pulse-on-time (T_{on})	90, 120, 150 μs
(D) Dielectric fluid (EDM oil)	No powder, Mn powder, W powder
(E) Electrode material	Cu, CuCr, CuW
(F) Cryogenic of electrode material	WCT, SCT, DCT
(G) Workpiece material	Ti, Ti–5Al–2.5Sn, Ti–6Al–4V
(H) Cryogenic of workpiece material	WCT, SCT, DCT
Depth of cut	1.00 mm
Powder concentration	10 gm/l
Dielectric fluid	Ferrolac 3 M EDM Oil

2.4 Process parameters and experimental design

For the present study, eight input parameters on the basis of literature and pilot study were selected to evaluate their effect on the surface properties. Out of eight factors, seven factors such as: (1) peak current (I_p), (2) pulse-on-time (T_{on}), (3) dielectric fluid, (4) electrode material, (5) cryogenic treatment of electrode material, (6) workpiece material, and (7) cryogenic treatment of workpiece material were varied at three levels and only one factor pulse-off-time (T_{off}) was varied at two levels. The machining parameters used for the experiments are listed in Table 1. Therefore, L_{18} mixed type of orthogonal array ($2^1 \times 3^7$) was identified as the most appropriate for the present study (refer Table 2). L_{18}OA has a special characteristic that the two way interaction between the control parameters is partially confounded with various columns. Hence, their impact on the main effect of the input parameters under considerations is minimized [25]. Each experiment was repeated twice; hence, all the 54 experiments were performed in a completely randomized fashion to minimize the effect of noise to the maximum extent. The value of micro-hardness obtained after each run and their calculated S/N ratios are summarized in Table 3.

2.5 Equipments

After the experimentation, all the machined samples were cleaned with acetone solution. The micro-hardness was measured using a digital display, micro-hardness tester (model: HVS-1000B). The indentations were made using a diamond indenter of pyramid shape under a test force of 9.807 N and dwell time of 10 s. The machined surface after each trial was examined using SEM (model JEOL, JSM-6610LV) for microstructure analysis along with energy-dispersive X-ray spectrometer (EDX) to know the weight percentage of different migrated elements on machined samples. XRD profiles were examined at different angles

2638

J Braz. Soc. Mech. Sci. Eng. (2017) 39:2635–2648

Table 2 L_{18} ($2^1 \times 3^7$) experimental design matrix with machining parameters

Trial no	Machining parameters								Trial run Condition
	A	B	C	D	E	F	G	H	
	T_{off} (μs)	Current (A)	T_{on} (μs)	Dielectric with powder	Electrode	Cryo of electrode	Work piece	Cryo of work piece	
1.	A1 = 30	B1 = 6	C1 = 90	D1 = No	E1 = Cu	F1 = WCT	G1 = Ti15	H1 = WCT	$A_1B_1C_1D_1E_1F_1$ G_1H_1
2.	A1 = 30	B1 = 6	C2 = 120	D2 = Mn	E2 = CuCr	F2 = SCT	G2 = Ti21	H2 = SCT	$A_1B_1C_2D_2E_2F_2$ G_2H_2
3.	A1 = 30	B1 = 6	C3 = 150	D3 = W	E3 = CuW	F3 = DCT	G3 = Ti31	H3 = DCT	$A_1B_1C_3D_3E_3F_3$ G_3H_3
4.	A1 = 30	B2 = 10	C1 = 90	D1 = No	E2 = CuCr	F2 = SCT	G3 = Ti31	H3 = DCT	$A_1B_2C_1D_1E_2F_2$ G_3H_3
5.	A1 = 30	B2 = 10	C2 = 120	D2 = Mn	E3 = CuW	F3 = DCT	G1 = Ti15	H1 = WCT	$A_1B_2C_2D_2E_3F_3$ G_1H_1
6.	A1 = 30	B2 = 10	C3 = 150	D3 = W	E1 = Cu	F1 = WCT	G2 = Ti21	H2 = SCT	$A_1B_2C_3D_3E_1F_1$ G_2H_2
7.	A1 = 30	B3 = 14	C1 = 90	D1 = No	E1 = Cu	F3 = DCT	G2 = Ti21	H3 = DCT	$A_1B_3C_1D_2E_1F_3$ G_2H_3
8.	A1 = 30	B3 = 14	C2 = 120	D3 = W	E2 = CuCr	F1 = WCT	G3 = Ti31	H1 = WCT	$A_1B_3C_2D_3E_2F_1$ G_3H_1
9.	A1 = 30	B3 = 14	C3 = 150	D1 = No	E3 = CuW	F2 = SCT	G1 = Ti15	H2 = SCT	$A_1B_3C_3D_1E_3F_2$ G_1H_2
10.	A2 = 45	B1 = 6	C1 = 90	D3 = W	E3 = CuW	F2 = SCT	G2 = Ti21	H1 = WCT	$A_2B_1C_1D_3E_3F_2$ G_2H_1
11.	A2 = 45	B1 = 6	C2 = 120	D1 = No	E1 = Cu	F3 = DCT	G3 = Ti31	H2 = SCT	$A_2B_1C_2D_1E_1F_3$ G_3H_2
12.	A2 = 45	B1 = 6	C3 = 150	D2 = Mn	E2 = CuCr	F1 = WCT	G1 = Ti15	H3 = DCT	$A_2B_1C_3D_2E_2F_1$ G_1H_3
13.	A2 = 45	B2 = 10	C1 = 90	D2 = Mn	E3 = CuW	F1 = WCT	G3 = Ti31	H2 = SCT	$A_2B_2C_1D_2E_3F_1$ G_3H_2
14.	A2 = 45	B2 = 10	C2 = 120	D3 = W	E1 = Cu	F2 = SCT	G1 = Ti15	H3 = DCT	$A_2B_2C_2D_3E_1F_2$ G_1H_3
15.	A2 = 45	B2 = 10	C3 = 150	D1 = No	E2 = CuCr	F3 = DCT	G2 = Ti21	H1 = WCT	$A_2B_2C_3D_1E_2F_3$ G_2H_1
16.	A2 = 45	B3 = 14	C1 = 90	D3 = W	E2 = CuCr	F3 = DCT	G1 = Ti15	H2 = SCT	$A_2B_3C_1D_3E_2F_3$ G_1H_2
17.	A2 = 45	B3 = 14	C2 = 120	D1 = No	E3 = CuW	F1 = WCT	G2 = Ti21	H3 = DCT	$A_2B_3C_2D_1E_3F_1$ G_2H_3
18.	A2 = 45	B3 = 14	C3 = 150	D2 = Mn	E1 = Cu	F2 = SCT	G3 = Ti31	H1 = WCT	$A_2B_3C_3D_2E_1F_2$ G_3H_1

along with X'Pert High Score Plus and Origin Pro 8 software to investigate the significant material transfer from the dielectric as well as electrode on the work surface either in free form and/or in compound form. The surface roughness of selected machined samples were measured in terms of arithmetic average deviation of the assessed profile (R_a) with MITUTOYO Surface Roughness Tester (model: Surftest SJ-400) at a cut of length of 0.8 mm. The machined samples were cleaned with acetone solution and etched with Kroll's reagent (5 ml hydrofluoric acid, 10 ml nitric acid and 85 ml distilled water) for microscopic analysis.

3 Analysis of experimental results

Here, the objective of the study was to maximize the value of surface hardness. Therefore, "higher-the-better" type of *S/N* ratio was selected and used for transforming the raw data of 54 samples. The average values by factor levels of raw data and *S/N* data are shown in Table 4. The main effects plots of raw data and *S/N* data on various factors are shown in Fig. 2a–h.

Outcomes of the analysis of variance (ANOVA) make it feasible to find out significance of parameters and their

Table 3 Observed micro-hardness (HVN) and calculated S/N ratios (dB)

Exp. no.	Micro-hardness of machined samples				Before machining	Improvement (%)	S/N ratios
	R1	R2	R3	Average			
1.	393	412	352	385.667	270	42.85	51.667
2.	432	397	425	418.000	310	34.85	52.406
3.	438	435	472	448.333	366	22.48	53.014
4.	465	445	425	445.000	366	21.58	52.949
5.	443	510	465	472.667	270	75.07	53.447
6.	482	465	502	483.000	310	55.80	53.666
7.	517	508	522	515.667	320	61.15	54.246
8.	562	610	548	573.333	315	82.00	55.141
9.	495	557	527	526.333	272	93.50	54.395
10.	457	437	445	446.333	305	46.33	52.989
11.	465	481	427	457.667	340	34.62	53.178
12.	442	415	435	430.667	287	50.07	52.674
13.	527	490	538	518.333	340	52.44	54.271
14.	475	517	510	500.667	287	74.45	53.973
15.	526	510	465	500.333	305	64.03	53.949
16.	540	515	535	530.000	272	94.85	54.480
17.	582	615	602	599.667	320	87.40	55.552
18.	592	602	620	604.667	315	91.96	55.626

$\overline{T_{MH}}$ = Overall mean of MH = 492 HVN, mean of S/N ratio m = 53.757

R1, R2, and R3 represent the repetition of the experiments

Table 4 Average values by factor levels of raw data and S/N data for micro-hardness

Control factors	Raw data (HVN)			S/N ratio (dB)		
	Level 1	Level 2	Level 3	Level 1	Level 2	Level 3
(A) Pulse-off-time, T_{off} (μs)	474.2	509.8	–	53.44	54.08	–
(B) Peak current, I_p (A)	431.1	486.7	558.3	52.65	53.71	54.91
(C) Pulse-on-time, T_{on} (μs)	473.5	503.7	498.9	53.43	53.95	53.89
(D) Dielectric fluid (EDM oil)	485.8	493.3	496.9	53.62	53.78	53.88
(E) Electrode material	491.2	482.9	501.9	53.73	53.60	53.94
(F) Cryogenics of electrode	498.4	490.2	487.4	53.83	53.72	53.72
(G) Workpiece material	474.3	493.8	507.9	53.44	53.80	54.03
(H) Cryogenics of workpiece	497.2	488.9	490.0	53.80	53.73	53.73

effect on performance characteristic. The ANOVA results for S/N data and raw data (means) are shown in Tables 5 and 6, respectively. The ANOVA results listed in Tables 5 and 6 indicates that the significant process parameters are current, pulse-off-time, pulse-on-time, workpiece, and electrode material. From ANOVA results (Tables 5 and 6), peak current was observed as the most significant factor with a percent contribution (PC) of 77 % that highly affecting the micro-hardness followed by a pulse-off-time with a PC of 9.3 %. Pulse-on-time is another important factor, which affecting the micro-hardness with a PC of 4.8 %.

4 Results and discussion

4.1 Micro-hardness

The values of micro-hardness for all machining tests are presented in Table 3. The micro-hardness for all the 54 values were obtained in the range of 352–620 HVN, while overall mean of micro-hardness 492 (HVN) was observed. The micro-hardness of all work samples before machining was also measured and the values are presented in the same Table 3. It is evident from Table 3 that the improvement in

Fig. 2 Effect of input parameters on micro-hardness: **a** effect of pulse-off-time; **b** effect of peak current; **c** effect of pulse-on-time; **d** effect of dielectric fluid, with manganese and tungsten powder; **e** effect of electrode material; **f** effect of cryogenic treatment of electrode material; **g** effect of different titanium alloy workpiece material and **h** effect of cryogenic treatment of different titanium alloy workpiece materials
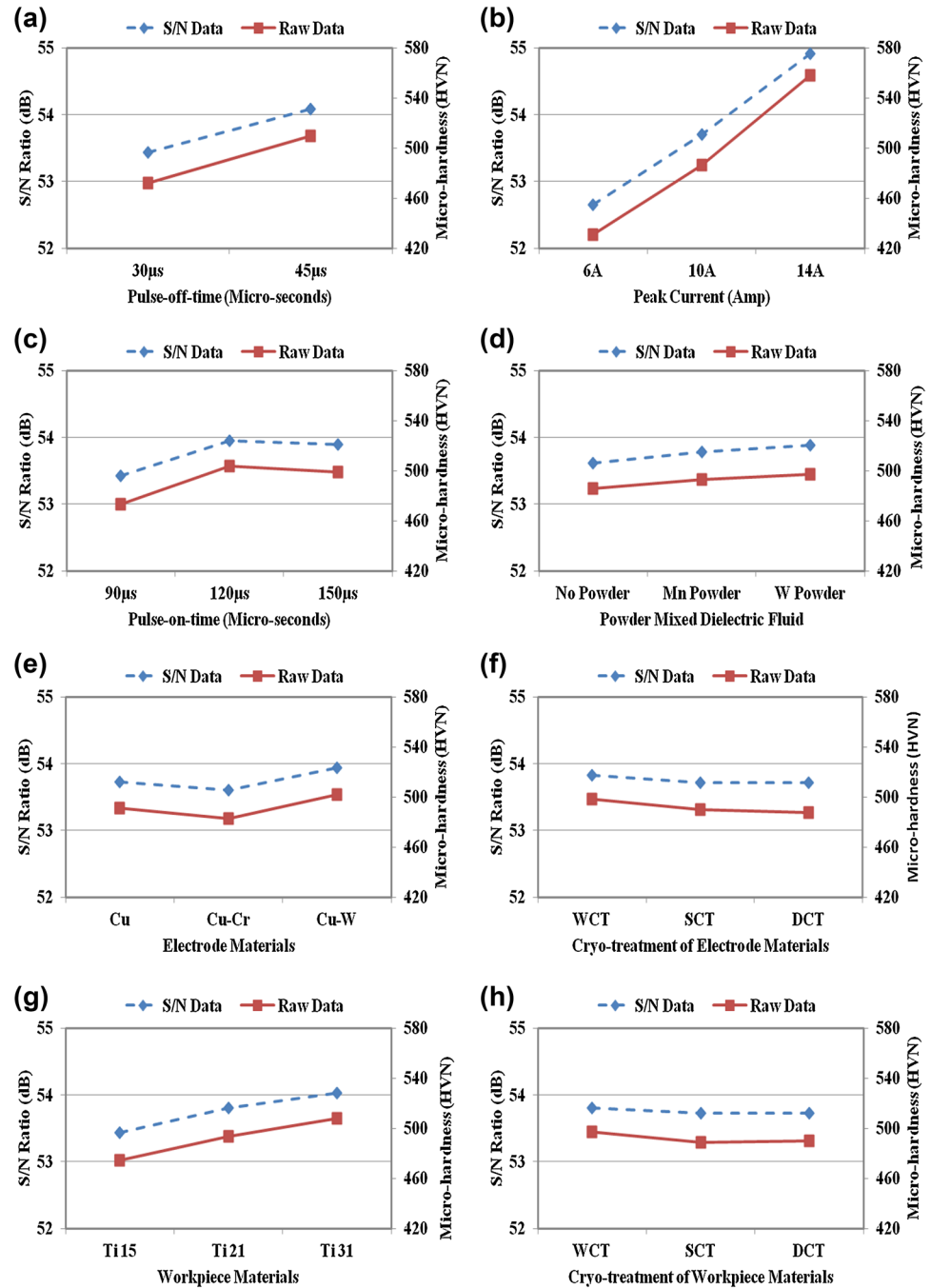
surface hardness after EDM was observed in the range of 21.58–94.85 %.

It has also been observed in Fig. 2a, b that by increasing peak current and pulse-off-time from 30 μs to 45 μs, the micro-hardness of machined part increases sharply due to excessive heating and quenching. While longer pulse-on-time (120–150 μs) reduces the micro-hardness as indicated in Fig. 2c. In EDM process, electrical discharge energy is totally dependent on process parameters such as peak current and duration of time, because these parameters have

a significant effect on hardness. Increase in peak current increases the available discharge energy during EDM process, increased the temperature at a high level, which helps in increasing the rate of melting and vaporization, thus, more metal re-solidifies on the machined surface [6, 10]. It means, higher the peak current, higher would be the metal deposition rate, and hence, higher would be the micro-hardness in expense of surface finish. In EDM, material will be melted away from the tool surface during pulse-on-time and deposited during pulse-off-time. Hence, with

Table 5 ANOVA results for micro-hardness (S/N ratio)

Control factors	DOF	Seq.SS	F value	%PC	Remarks	Best level
(A) Pulse-off-time, T_{off} (µs)	1	1.842	298.07	9.33	**	$A_2 = 45$ µs
(B) Peak current, I_p (A)	2	15.233	1232.35	77.15	***	$B_3 = 14$ A
(C) Pulse-on-time, T_{on} (µs)	2	0.951	76.94	4.82	**	$C_2 = 120$ µs
(D) Dielectric fluid (EDM oil)	2	0.210	17.01	1.06	x	$D_3 =$ W powder
(E) Electrode material	2	0.365	29.54	1.85	*	$E_3 =$ CuW
(F) Cryogenics of electrode	2	0.046	3.74	0.23	x	$F_1 =$ WCT
(G) Workpiece material	2	1.065	86.14	5.40	**	$G_3 =$ Ti31
(H) Cryogenics of workpiece	2	0.019	1.56	0.10	x	$H_1 =$ WCT
Error	2	0.012		0.06		
Total	17	19.744				

*** Most significant, ** significant, * less significant, x not significant

Table 6 ANOVA results for micro-hardness (means)

Control factors	DOF	Seq. SS	F value	%PC	Remarks	Best level
(A) Pulse-off-time, T_{off} (µs)	1	5700.7	78.44	9.00	**	$A_2 = 45$ µs
(B) Peak current, I_p (A)	2	48,771.9	335.56	77.05	***	$B_3 = 14$ A
(C) Pulse-on-time, T_{on} (µs)	2	3154.9	21.71	4.98	**	$C_2 = 120$ µs
(D) Dielectric fluid (EDM oil)	2	389.6	2.68	0.62	x	$D_3 =$ W powder
(E) Electrode material	2	1095.0	7.53	1.73	*	$E_3 =$ CuW
(F) Cryogenics of electrode	2	393.9	2.71	0.62	x	$F_1 =$ WCT
(G) Workpiece material	2	3407.6	23.44	5.38	**	$G_3 =$ Ti31
(H) Cryogenics of workpiece	2	242.2	1.67	0.38	x	$H_1 =$ WCT
Error	2	145.3		0.24		
Total	17	63,301.2				

*** Most significant, ** significant, * less significant, x not significant

longer on-time, rate of melting from tool/workpiece surface increases, it means material deposition on the machined surface increases during off-time, resulting in higher micro-hardness. However, the longer on-time causes arcing and makes the machining process unstable, thus, decreasing the surface hardness [6]. As indicated in Fig. 2c, micro-hardness decreases as the pulse-on-time extended from 120–150 µs, because the amount of discharge energy is reduced due to expansion of plasma channel and this state has a negative effect on hardness. As a result, rate of melting and vaporization decreases. This issue leads to decrease in the amount of metal deposited on the machined surface, thus, reduced the surface hardness. The same result was reported by Kumar et al. [15].

The trend indicated in Fig. 2d shows the influence of powder suspended dielectric medium on the surface hardness. The plot shows that the powder mixed dielectric either Mn or W had less effect on surface hardness as compared to the other process parameters. It may be possible that the powder concentration (10 g/l) did not significantly affect the hardness. However, tungsten powder mixed dielectric gives the higher hardness as compared to manganese powder as shown in Fig. 2d.

According to Fig. 2e and ANOVA results (Tables 5, 6), the less effect of electrode material was observed (PC 1.85 %). The copper-tungsten electrode produces a surface with higher hardness compared with the copper and copper-chromium electrode. The work material type and their properties significantly affected the machined parts' hardness as observed from Fig. 2g and ANOVA results presented in Tables 5 and 6. The workpiece material contributes on the micro-hardness with a PC of 5.40 %. Lower value of surface hardness was observed with Ti 15 alloy, while higher value of micro-hardness with Ti–6Al–4V alloy was obtained during the EDM process. It may be happening due to the presence of alloying elements in the alloy. Negligible effect of cryogenic-treatment of workpiece/electrode material was observed on the micro-hardness as can be seen from ANOVA results. The observed results were plotted to examine the variation trend of micro-hardness with change in each input parameter.

4.2 Macro-model for micro-hardness

Referring Fig. 2a–h, it is concluded that higher values of micro-hardness can be achieved when without cryo-treated

TITAN 31 (Ti–6Al–4V) titanium alloy work material machined with copper-tungsten electrode (WCT) using a higher value of pulse-off-time (45 μs), the highest value of current (14 A), medium level of pulse-on-time (120 μs), and tungsten powder mixed dielectric fluid. Therefore, the optimum combination of input process parameters for is $(A_2B_3C_2D_3E_3F_1G_3H_1)$.

Since, this observed combination of process variables did not exist in OA, therefore, a set of three confirmation experiments was conducted using optimal combination. The results obtained after conducting the confirmation experiments must fall within the 95 % confidence interval ($\alpha = 0.05$). The Taguchi methodology for predicting the mean performance and determination of confidence interval for predicting mean has been applied.

For micro-hardness response, the overall mean value of the observed results is: $\overline{T} = 492$ HVN.

The predicted optimum value with significant factor of MH is calculated as using Eq. (1) (Table 6)

$$\begin{aligned} \text{MH}_{\text{opt}} &= \left(\overline{T}A_2 + \overline{T}B_3 + \overline{T}C_2 + \overline{T}E_3 + \overline{T}G_3\right) - \left(4\overline{T}\right) \\ &= 613.6 \text{ HVN}, \end{aligned} \tag{1}$$

where $\overline{T}$ is the overall average values of micro-hardness, A_2 is the average value of pulse-off-time at second level, B_3 is the average value of peak current at the third level, C_2 is the average value of pulse-on-time at the second level, E_3 is the average value of electrode material at the third level, and G_3 is the average value of workpiece material at third level.

According to the 95 % confidence interval of the population (CI) was calculated using following Eq. (2) [25]:

$$\text{CI} = \pm\sqrt{\frac{F_\alpha, (f_1 f_2) \times V_e}{n_{\text{eff}}}}, \tag{2}$$

where $F_\alpha (f_1, f_2)$ is the variance ratio for DOF f_1 and f_2 at the level of significance α. The confidence level is $(1 - \alpha)$. α is the 0.05, risk. f_1 is the degree of freedom for mean, which is always $= 1$. $f_2 =$ degree of freedom for error term $= 8$. n_{eff} is the number of tests under that condition participating factors. From F table at 95 % confidence level $F_\alpha = 5.3177 V_e$ is the pooled error variance for MH $= 146.375$ (Table 6). N is the total number of trials $= 18$.

$$N_{\text{eff}} = \frac{N}{1 + \text{DOF}} = 18/(1 + 9) \tag{3}$$

The effective number of replications is N_{eff} using Eq. (3) $= 1.8$.

Thus, the calculated confidence interval, CI_{CE} for MH $= \pm 20.80$.

Therefore, the 95 % CI of the estimated mean of MH is given by 613.6 ± 20.80 HVN.

Hence, estimated MH is given as $592.8 < 613.6 < 634.4$ HVN.

From the confirmation experiments, the average value of MH obtained at this setting of $(A_2B_3C_2D_3E_3F_1G_3H_1)$ was 635.667 HVN, which is very close to the theoretical predicted value. Hence, the validity of the experimental design is confirmed.

5 Metallographic analysis

5.1 Analysis based on SEM micrographs

The surface morphology of the machined surface after EDM is mainly affected by current and pulse-on-time. With the increase in current and pulse-on-time, high discharge energy is supplied to the machining zone for long duration, thus increasing the melting and vaporization rate, leaving a crater on the surface. Further, due to high discharge energy, impulsive force also increases, which contributes to formation of deeper and larger crater size which causes rough finish [6]. Also, due to high discharge energy surface defects such as globules of debris particles, pin-holes, micro-pores, melted particles, craters of different sizes, surface cracks are noticed on the machined surfaces, resulted in a poor surface finish. (Refer Figs. 3, 4, 5). Due to the repeated heating and cooling, stresses are developed and when these stresses are increased cracks are formed on the machined surfaces [6]. At higher current and pulse-on-time, wider/deeper cracks were formed on machined surface.

For the purpose of analysis, six trials (two for each material) with the lowest and the highest current setting, namely (1) 6 A and (2) 14 A, were analyzed in detail and are presented below.

SEM micrographs of the three different machined workpiece surfaces such as Ti alloy (TITAN 15 ASTM Grade 2), Ti–5Al–2.5Sn (TITAN 21 ASTM Grade 6), and Ti–6Al–4V (TITAN 31 ASTM Grade 5) at different machining conditions were examined using SEM analyzer. Figures 3, 4, and 5a, b show the microstructure of six machined samples, two for each workpiece at lower and higher value of peak current. SEM micrograph of DCT Ti alpha alloys machined with copper-chromium electrodes (Cu–Cr) in manganese powder mixed dielectric fluid at 6A current, 150 μs $T_{\text{on,}}$ and 45 μs T_{off} is shown in Fig. 3a. The figure shows the formation of thin surface cracks and sporadic tiny holes on the surface. A recast layer can also be seen on the workpiece surface. Small size debris and re-solidified particles are observed on the surface. Figure 3b shows the micrograph of SCT titanium machined with DCT Cu–Cr electrodes when tungsten powder was mixed into the dielectric fluid at 14 A current, 90 μs T_{on}, and 45 μs T_{off}. More micro-pores can be clearly seen on the surface, in addition to, surface cracks and tiny holes. The large crater size was observed as well as debris particles result in higher surface roughness due to higher current 14 A.
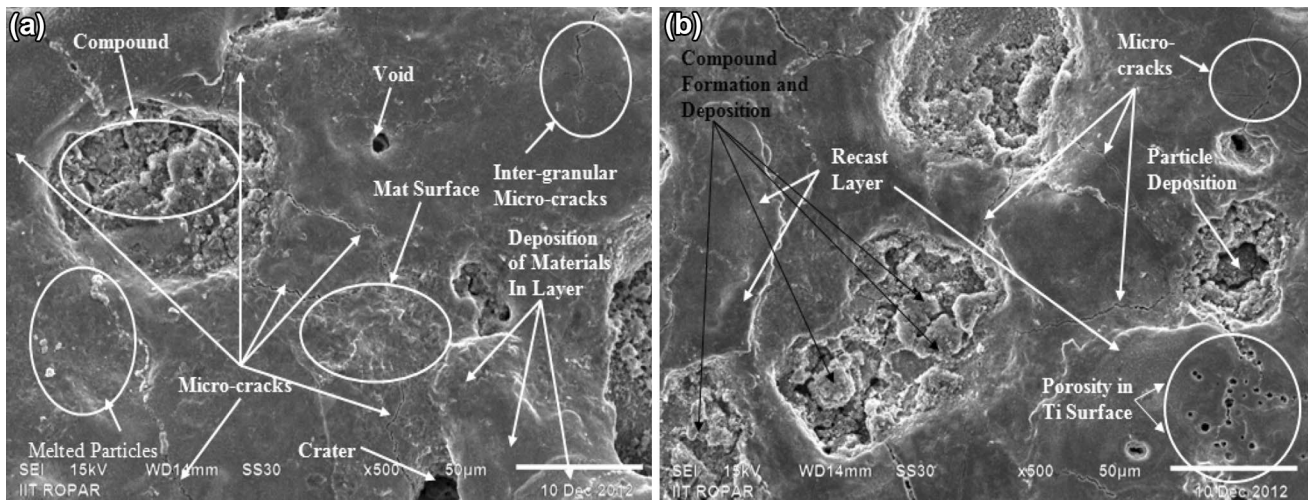
Fig. 3 a SEM micrograph of DCT Ti alloy machined with WCT Cu–Cr electrode in Mn powder mixed dielectric (Ip 6 A, T_{on} 150 μs, T_{off} 45 μs) for exp. no. 12. **b** SEM micrograph of SCT Ti alloy machined with DCT Cu–Cr electrode in W powder mixed dielectric (Ip 14 A, T_{on} 90 μs, T_{off} 45 μs) for exp. no. 16
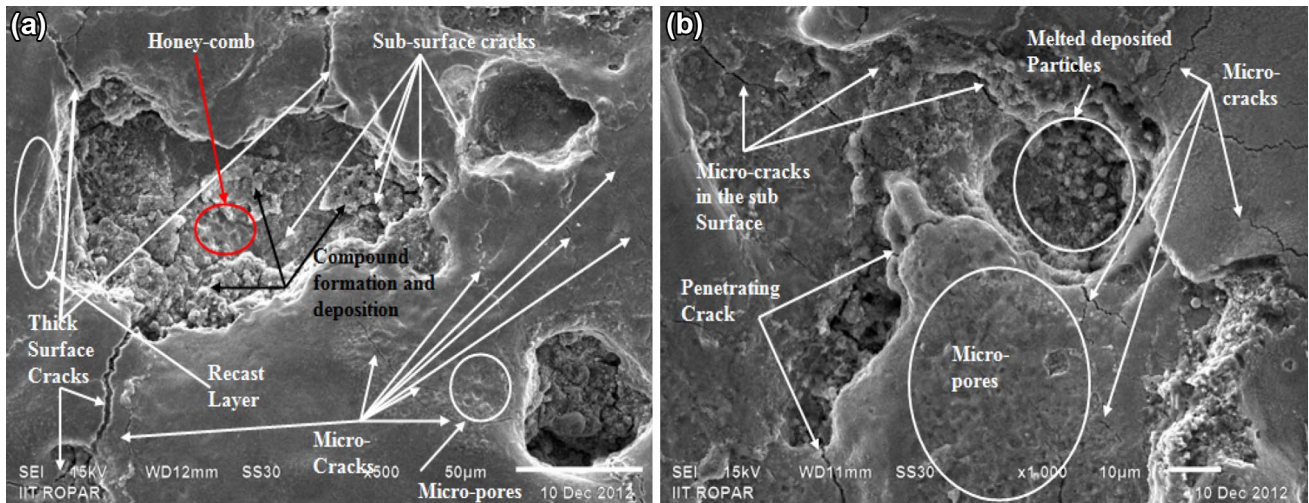
Fig. 4 a SEM micrograph of SCT Ti–5Al–2.5Sn alloy machined with SCT Cu–Cr electrode in Mn powder mixed dielectric (Ip 6 A, T_{on} 120 μs, T_{off} 30 μs) for exp. no. 2. **b** Figure 6.17: SEM micro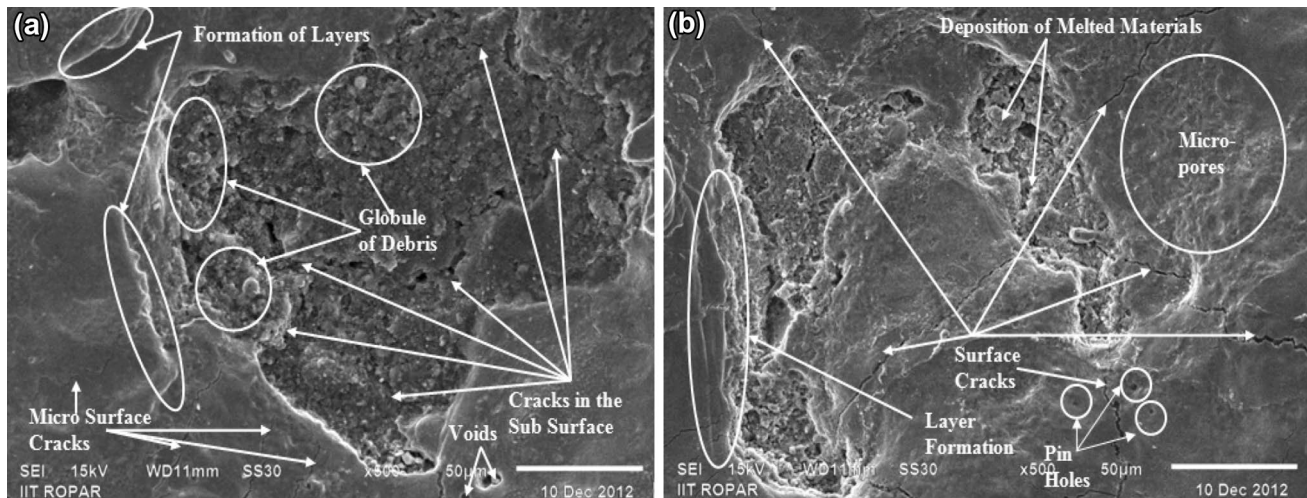graph of DCT Ti–5Al–2.5Sn alloy machined with WCT Cu–W electrode in EDM oil dielectric (Ip 14 A, T_{on} 120 μs, T_{off} 45 μs) for 17 exp. no

The debris particles were not completely removed from the machining area. Thermal stresses are developed on the work material due to high current, thus, cracks are observed on the surface. The machined surface also showed a poorer surface finish 5.48 μm (R_a) at 14 A current compared to the one obtained at 6 A with 4.31 μm (R_a). Wider surface cracks were observed at 14 A current compared to the 6 A current because of high discharge energy. The difference between the surface topography of two machined samples of Ti alloy can be clearly seen in Fig. 3a, b.

Figure 4a, b presents the machining characteristics of alpha group Ti–5Al–2.5Sn (TITAN 21) alloy machined

samples. Figure 4a presents the SEM picture of SCT Ti–5Al–2.5Sn machined in the presence of suspended manganese powder in EDM dielectric oil by SCT Cu–Cr electrode. The process settings were I_p 6 A, T_{on} 120 μs, and T_{off} 30 μs. Surface cracks are clearly seen on the surface. More micro-pores are visible on the machined part.

Further, Fig. 4b presents the SEM picture of DCT Ti–5Al–2.5Sn which was machined with Cu-W electrode with machine variables I_p 14 A, T_{on} 120 μs, and T_{off} 45 μs when no powder has been added to the dielectric fluid. By increasing the current from 6 to 14 A, the amplitude of discharge energy in between the machining zone is also

Fig. 5 a SEM micrograph of DCT Ti–6Al–4V alloy machined with DCT Cu–W electrode in W powder mixed dielectric (Ip 6 A, T_{on} 150 μs, T_{off} 30 μs) for exp. no. 3. **b** SEM micrograph of WCT Ti–6Al–2.4V alloy machined with SCT Cu electrode in Mn powder mixed dielectric (Ip 14 A, T_{on} 150 μs, T_{off} 45 μs) for exp. no. 18

increased, thus, removing more metal from the workpiece as well as increasing the electrode wear and roughness because of a deeper and larger crater. The machined surface also showed rough surface finish 6.42 μm (R_a) at 14 A current compared to the one obtained at 6 A with 5.23 μm (R_a). When contraction stress increases beyond the ultimate tensile stress of the material within the white layer, surface cracks are developed [6, 24].

Figure 5a, b presents the typical micrographs of the EDMed surface of alpha–beta Ti–6Al–4V. The DCT Ti–6Al–4V work specimen was machined using DCT Cu–W tool with W powder mixed with dielectric at a 6A I_p, 150 μs T_{on}, and 30 μs T_{off}. The typical SEM view of the machined surface has been shown in Fig. 5a. From the study of micrograph, damaged surface is observed due to the surface defects such as surface cracks, pin-holes, globules of debris and formation of recast layer, melted drops, and craters, resulting in an uneven surface texture. Further, the same material without cryogenic treatment was machined by mixing manganese powder in dielectric with an SCT Cu electrode at 14A I_p, 150 μs T_{on}, and 45 μs T_{off}. Figure 5b shows the micro-structural view of the sample. Again, surface cracks, micro-pores, and globules are observed on the surface. Surface finish of Ti–6Al–4V machined sample obtained 6.81 μm (R_a) at 14 A current compared to obtain at 6 A current surface finish 4.89 μm (R_a).
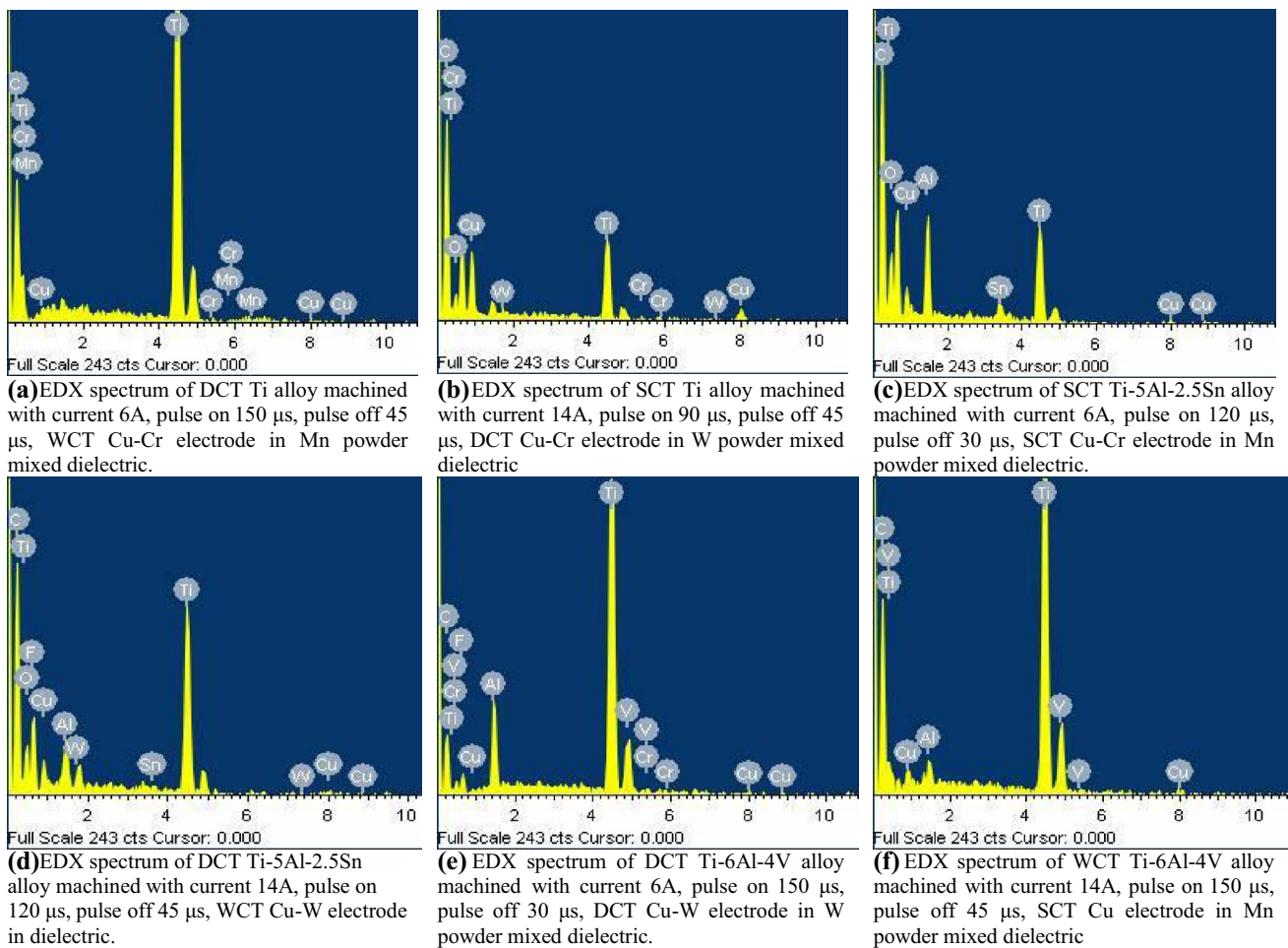
5.2 Analysis based on EDX

The composition analysis of the machined surfaces was studied using EDX analyzer. The EDX examination confirmed the presence of the parent metal and migration chemical elements from the electrode and dielectric fluid,

as shown in Fig. 6a–f. Migration of carbon (C) after the decomposition of dielectric fluid due to high temperature has been observed in large percentages. The EDX analysis showed that due to the high thermal energy, material gets melted and evaporated from the surface of workpiece and the electrode. Thus, detached material from workpiece may deposit on the electrode surface or vice versa. Moreover, the material may also migrate from the dielectric to the workpiece as well as electrode. Figure 6a, b shows the EDX analysis for the two trials described above for Ti. These figures show the peaks of the different elements present on the machined surface. The maximum peak heights of titanium are clearly visible on the EDX spectra followed by carbon. EDX analysis was conducted on the workpiece surface at five spectrums. The average weight percentage of different elements is given in Table 7. Copper-chromium electrode has been used for the machining of titanium with manganese (Mn) and tungsten (W) powder. The EDX spectra shows peaks of Cu and Cr migrated from the electrode as well as Mn and W migrated from the powder mixed dielectric fluid.

Figure 6c, d shows the EDX spectra of the two cases (trial 2 and 7) described above and shows the peaks of the different elements present in the machined samples. Copper and tungsten are transferred from the tool to the workpiece as can be seen in figure. Table 7 represents the weight percentage of different elements.

The EDX pattern for the two trials is shown in Fig. 6e, f for trial 3 and 18. Like before, the migration of different elements from the electrode and dielectric fluid can be seen in the plots. Table 7 shows the average weight percentage of different elements for the two trial conditions described above.
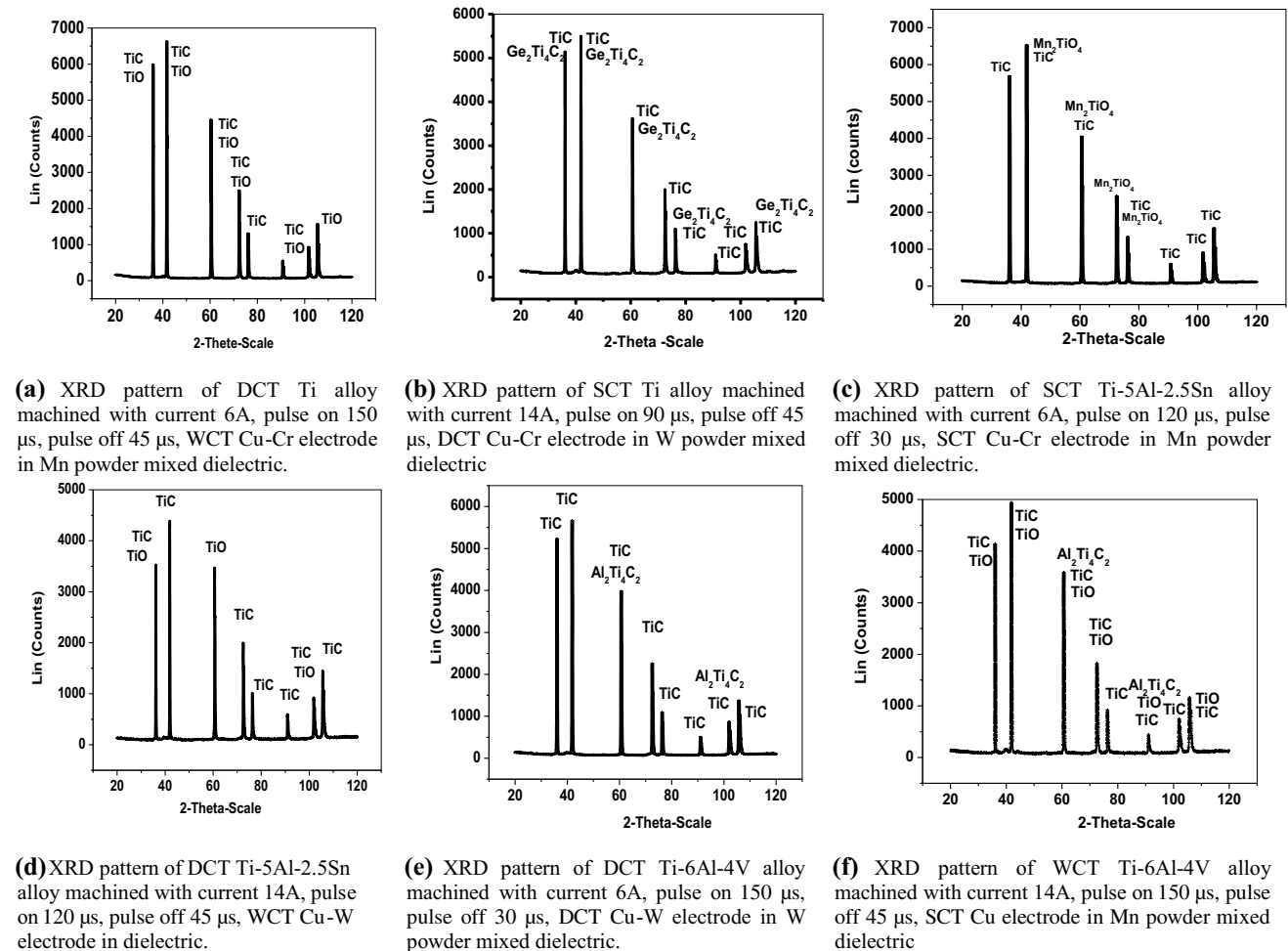
(a) EDX spectrum of DCT Ti alloy machined with current 6A, pulse on 150 μs, pulse off 45 μs, WCT Cu-Cr electrode in Mn powder mixed dielectric.

(b) EDX spectrum of SCT Ti alloy machined with current 14A, pulse on 90 μs, pulse off 45 μs, DCT Cu-Cr electrode in W powder mixed dielectric

(c) EDX spectrum of SCT Ti-5Al-2.5Sn alloy machined with current 6A, pulse on 120 μs, pulse off 30 μs, SCT Cu-Cr electrode in Mn powder mixed dielectric.

(d) EDX spectrum of DCT Ti-5Al-2.5Sn alloy machined with current 14A, pulse on 120 μs, pulse off 45 μs, WCT Cu-W electrode in dielectric.

(e) EDX spectrum of DCT Ti-6Al-4V alloy machined with current 6A, pulse on 150 μs, pulse off 30 μs, DCT Cu-W electrode in W powder mixed dielectric.

(f) EDX spectrum of WCT Ti-6Al-4V alloy machined with current 14A, pulse on 150 μs, pulse off 45 μs, SCT Cu electrode in Mn powder mixed dielectric

Fig. 6 **a** EDX spectrum for trial 12 machined with condition $A_2B_1C_3D_2E_2F_1G_1H_3$. **b** EDX spectrum for trial 16 machined with condition $A_2B_3C_1D_3E_2F_3G_1H_2$. **c** EDX spectrum for trial 2 machined with condition $A_1B_1C_2D_2E_2F_2G_2H_2$. **d** EDX spectrum for trial 17 machined with condition $A_2B_3C_2D_1E_3F_1G_2H$. **e** EDX spectrum for trial 3 machined with condition $A_1B_1C_3D_3E_3F_3G_3H_3$. **f** EDX spectrum for trial 18 machined with condition $A_2B_3C_3D_2E_1F_2G_3H_1$

Table 7 Average weights (%) of different elements of three grades of titanium alloys

Elements	Average weight (%) of different elements					
	TITAN 15 (Ti)		TITAN 21 (Ti–5Al–5Sn)		TITAN 31 (Ti–6Al–4V)	
	Exp. 12	Exp. 16	Exp.02	Exp.17	Exp.3	Exp.18
C	28.978	34.884	24.07	36.532	38.39	41.474
O	5.938	5.128	5.508	11.126	7.708	5.328
Ti	64.674	48.732	65.102	25.954	31.852	47.456
Cu	0.07	2.718	0.542	0.674	1.20	1.698
Cr	0.112	0.11	0.016	–	0.108	0.166
Mn	0.232	–	–	–	–	0.036
W	–	0.282	–	6.612	0.808	–
Al	–	–	0.996	1.898	2.838	1.806
Sn	–	–	1.61	0.818	–	–
V	–	–	–	–	1.476	2.034
F	–	8.146	2.152	16.382	15.614	–
Total	100.00	100.00	100.00	100.00	100.00	100.00

(a) XRD pattern of DCT Ti alloy machined with current 6A, pulse on 150 μs, pulse off 45 μs, WCT Cu-Cr electrode in Mn powder mixed dielectric.

(b) XRD pattern of SCT Ti alloy machined with current 14A, pulse on 90 μs, pulse off 45 μs, DCT Cu-Cr electrode in W powder mixed dielectric

(c) XRD pattern of SCT Ti-5Al-2.5Sn alloy machined with current 6A, pulse on 120 μs, pulse off 30 μs, SCT Cu-Cr electrode in Mn powder mixed dielectric.

(d) XRD pattern of DCT Ti-5Al-2.5Sn alloy machined with current 14A, pulse on 120 μs, pulse off 45 μs, WCT Cu-W electrode in dielectric.

(e) XRD pattern of DCT Ti-6Al-4V alloy machined with current 6A, pulse on 150 μs, pulse off 30 μs, DCT Cu-W electrode in W powder mixed dielectric.

(f) XRD pattern of WCT Ti-6Al-4V alloy machined with current 14A, pulse on 150 μs, pulse off 45 μs, SCT Cu electrode in Mn powder mixed dielectric

Fig. 7 **a** XRD pattern for trial 12 machined with condition $A_2B_1C_3D_2E_2F_1G_1H_3$. **b** XRD pattern for trial 16 machined with condition $A_2B_3C_1D_3E_2F_3G_1H_2$. **c** XRD pattern for trial 2 machined with condition $A_1B_1C_2D_2E_2F_2G_2H_2$. **d** XRD pattern for trial 17 machined with condition $A_2B_3C_2D_1E_3F_1G_2H$. **e** XRD pattern for trial 3 machined with condition $A_1B_1C_3D_3E_3F_3G_3H_3$. **f** XRD pattern for trial 18 machined with condition $A_2B_3C_3D_2E_1F_2G_3H_1$

5.3 Analysis based on XRD

X-ray Diffraction (XRD) analysis was done using a Cu–kα source ($\lambda = 1.54060$ Å) over the 2θ range from 20° to 120°, at temperature of 25 °C. The XRD patterns for the two trials of Ti alloy machined at different parameters are presented in Fig. 7a, b. The pattern shows the presence of titanium-carbide (TiC) at 2θ values of 35.88, 41.678, 60.4246, 72.327, 76.0977, 90.749, and 101.727. The highest peak was observed at 2θ values 41.678 (Cu K-alpha). In addition to TiC, titanium oxide (TiO) phase is also observed on the machined surface at 2θ values 35.88, 41.678, 60.4246, 72.327, 90.749, 101.727, and 105.459. The TiC compounds have the highest score followed by the TiO as shown in Fig. 7a.

Moreover, some other compounds of very low score such as manganese–titanium–oxide (Mn_2TiO_4), zinc–titanium–oxide ($ZnTiO_3$), titanium–zinc–carbide (Zn_2Ti_4C), and

aluminum–titanium–carbide ($Al_2Ti_4C_2$) are noticed during the analysis and thus did not show in the XRD plot.

Figure 7b presents the XRD plot of SCT (Ti– grade 2) titanium workpiece machined with DCT copper-chromium electrode in tungsten powder mixed dielectric fluid at 14 A current. The hard black carbon compound TiC is observed in the XRD pattern of maximum score 72 at 2θ position 36.1085, 41.9016, 60.6360, 72.5331, 76.306, 101.938, and 105.649. Another compound germanium–titanium–carbide ($Ge_2Ti_4C_2$) with low score 7 is found at 2θ position 36.1085, 39.95, 41.9016, 60.6360, and 105.649. Further, traces of compounds nickel–titanium–oxide (Ni_3TiO_5), sodium–iron–titanium–oxide ($NaFeTiO_4$), sodium–titanium–oxide (Na_2TiO_3), copper–titanium–oxide ($CuTiO_3$), titanium–zinc–carbide (Zn_2Ti_4C), rutile (TiO_2), and titanium–oxide (TiO) are observed during the analysis. Due to the low intensity, all these compounds are not seen in XRD analysis.

The XRD patterns for the two trial conditions of Ti–5Al–2.5Sn alloy are shown in Fig. 7c, d. The XRD pattern of SCT Ti–5Al–2.5Sn alloy machined at I_p 6A, T_{on} 120 µs, and T_{off} 30 µs in the presence of suspended manganese powder in dielectric fluid using SCT copper–chromium electrode is shown in Fig. 7c. The carbides of Titanium and manganese–titanium–oxide can be seen on the XRD pattern due to the migration of carbon and manganese from dielectric fluid. Irrespective of these two, other compounds such as hongquite (TiO), potassium–titanium–oxide–fluoride (K_3TiOF_5), iron–titanium–oxide (FeTiO), sodium–iron–titanium–oxide (NaFeTiO$_4$), copper–titanium–oxide (CuTiO$_3$), rutile (TiO$_2$), and yttrium–titanium–oxide ($Y_2Ti_2O_7$) are noticed during the analysis. Due to the less intensity of these compounds, they cannot be seen in the XRD plot.

The XRD pattern of DCT Ti–5Al–2.5Sn machined with copper–tungsten electrode with machining parameters, I_p 14A, T_{on} 120 µs, and T_{off} 45 µs when no powder has been added to the dielectric fluid is presented in Fig. 7d. The XRD pattern indicates the formation of oxide and carbide of titanium (TiO and TiC) after machining. Titanium–carbide of black appearance is formed during the machining which is extremely hard particles similar to tungsten–carbides, which makes the parts more brittle. The TiC particle is formed by decomposition of carbon present in the dielectric fluid during machining. The decomposed carbon penetrates the machined surface. In addition to TiC compounds, XRD pattern in Fig. 7d confirms that the titanium oxide (Hongquite) phase occurs with layers dominated by the rutile phase formed on the work piece surface. Further, it is observed that the white TiO film sticks on the workpiece and does not get removed during machining. This film hinders the flow of current through the two electrodes [4]. Further, in addition to the above compound, some others, such as aluminum–titanium–carbide ($Al_2Ti_4C_2$), tin–titanium–carbide (SnTi$_2$C), manganese–titanium–oxide (Mn$_2$TiO$_4$), tin–titanium–tungsten–oxide (Sn$_2$TiWO$_7$), copper–titanium–oxide (Cu$_2$TiO$_3$), etc., are also observed in small proportion due to the low weight percentage of the elements.

The XRD pattern for the two trials of Ti–6Al–4V titanium alloy is shown in Fig. 7e, f. Figure 7e shows the XRD pattern of DCT Ti–6Al–4V alloy machined using DCT Cu–W tool when W powder was added into the dielectric fluid at a 6A I_p, 150 µs T_{on}, and 30 µs T_{off}. The XRD pattern indicates the formation of TiC which is a carbide form of titanium at 2θ positions 36.0653, 41.8732, 60.6512, 72.5821, 76.364, 91.066, 102.024, 105.819 with compound $Al_2Ti_4C_2$ at 60.6512 and 102.024. The other compounds such as calcite (CaCO$_3$), nickel–hydroxide–methoxide ($C_2H_{10}Ni_3O_6$), and gallium–titanium–carbide (Ga$_2$Ti$_4$C$_2$) have been confirmed, but have a very low wattage.

Similarly, Fig. 7f shows the XRD pattern of Ti–6Al–4V machined at 14A current. The black hard and brittle formation of TiC formed at 2θ positions 36.0512, 41.8612, 60.6404, 72.547, 76.364, 91.085, 102.099, 105.842. Formation of white TiO is observed at 36.0512, 41.8612, 60.6404, 72.547, 76.364, 91.085, 105.842 and $Al_2Ti_4C_2$ at a 2θ angle 60.6404 and 102.099. The low score of other compounds like Zn$_2$Ti$_4$C, Mn$_2$TiO$_4$, FeTiO, K_3TiOF_5, and Cu$_2$TiO$_3$ is noticed in the analysis.

Decomposed carbon from the dielectric EDM oil due to high temperature is precipitated on the machined surface either in free form or compound form. Different carbide compounds were observed in the analysis, especially, TiC and $Al_2Ti_4C_2$. The migrated carbon also sticks to the bottom surface of electrodes, thus reducing the discharge efficiency. The melting point and the boiling point of these titanium-carbide compounds are approximately 3160 °C (just twice of titanium) and 4820 °C, respectively, which increase the time for melting, boiling, and evaporation of materials and require the more discharge energy for machining, hence results in a decrease of the machining efficiency [4, 6]. Moreover, various oxide compounds also formed during this process, especially, TiO, which, acts as a barrier between the current flows, thus, reducing the machining efficiency. The reason of their formation is the interaction of titanium element of base material with soluble oxygen in a dielectric fluid. Due to this reason, base material elements interact with the cracked carbon as well as soluble oxygen, respectively; hence various phases/compounds in carbide or oxide form were produced on the machined specimen. This statement was also confirmed by the Jabbaripour et al. [10] in their study. Formation of TiC has a large score as compared to the TiO because the percentage of migrated carbon is much more as compared to the oxygen.

The weight % of this transferred carbon element is more as compared to the other elements which are transferred from the tool-electrode to the workpiece surface and vice versa. This transferred carbon interacts with the workpiece elements, e.g., the element, which has large percentage. Due to this phenomenon, TiC compound is formed with high score and produced on the machined surface as shown in the XRD patterns. The presence of other elements has a low percentage in the composition of the workpiece; hence, various compounds of low score are produced on the machined surface.

6 Conclusions

The main aim of this study is to experimentally analyze and investigate the effect of different process parameters on surface properties during EDM of three grades of titanium

alloys with three different electrode materials. Surface modification of machined parts was measured in terms of micro-hardness. From the experimental results, it has been found that significant amount of different materials transfer on the machined surface from the powder added dielectric liquid as well as from the electrode material under different machining conditions which modify the chemistry of the machined surface and increased hardness of machined surface. In this study, the percentage of carbon is significantly increased (Table 7) which resulted in the formation of various carbide compounds, resulted in an improvement in micro-hardness. In addition to carbon, migration of other elements such as oxygen, copper, manganese, tungsten, and chromium were also observed in the EDX spectrum, which further resulted in the formation of different types of chemical compounds on the machined surface. The experimental results showed that micro-hardness increased up to 94.85 %. The SEM images show the various surface defects such as micro-cracks, micro-pores, tiny holes, craters of different size, globules of debris, and recast layer on the machined specimens. At lower current and pulse-on-time better surface characteristics may be obtained as compared with higher current and pulse-on-time, due to low discharge energy for less pulse duration. The maximum micro-hardness 635.67 HVN was observed at the optimum setting of parameters. This study has added more insight in the surface modification of different grades of titanium alloy through material transfer mechanism by EDM which is still in the state of research.

References

1. Ezugwu EO, Wang ZM (1997) Titanium alloys and their machinability-a review. J Mater Process Technol 68:262–274
2. Kao JY, Tsao CC, Wang SS, Hsu C (2010) Optimization of the EDM parameters on machining Ti–6Al–4V with multiple characteristics. Int J Adv Manuf Technol 47:395–402
3. Lin YC, Yan BH, Chang YS (2000) Machining characteristics of Titanium alloy (Ti–6Al–4V) using a combination process of EDM with USM. J Mater Process Technol 104:171–177
4. Yan BH, Chang GW, Chang JH, Hsu RT (2004) Improving electrical discharge machined surfaces using magnetic abrasive finishing. Mach Sci Technol An Int J 8(1):103–118
5. Yan BH, Tsai HC, Huang FY (2005) The effect in EDM of a dielectric of a urea solution in water on modifying the surface of Titanium. Int J Mach Tools Manuf 45:194–200
6. Hascalik A, Caydas U (2007) Electric discharge machining of Titanium alloy (Ti–6Al–4V). Appl Surf Sci 253:9007–9016
7. Pardhan BB, Masanta M, Sarkar BR, Bhattacharyya B (2009) Investigation of electro-discharge micro-machining of Titanium super alloy. Int J Adv Manuf Technol 41(11–12):1094–1106
8. Kibria G, Sarkar B, Pradhan BB, Bhattacharyya B (2010) Comparative study of different dielectrics for micro-EDM performance during microhole machining of Ti–6Al–4V alloy. Int J Adv Manuf Technol 48:557–570
9. Lin YC, Lee HS (2008) Machining characteristics of magnetic force-assisted EDM. Int J Mach Tools Manuf 48:1179–1186
10. Jabbaripour B, Sadeghi MH, Faridvand S, Shabgard MR (2012) Investigating the effects of EdM parameters on surface integrity, MRR and TWR in machining of Ti–6Al–4V. Mach Sci Technol Int J 16:419–444
11. Chow HM, Yan BH, Huang FY, Hung JC (2000) Study of added powder in kerosene for the micro-slit machining of titanium alloy using electro-discharge machining. J Mater Process Technol 101:95–103
12. Batish A, Bhattacharya A, Singla VK, Singh G (2012) Study of material transfer mechanism in die steels using powder mixed electric discharge machining. Mate Manuf Process 27:449–456
13. Kumar A, Maheshwari S, Sharma C, Beri N (2010) A study of multi objective parametric optimization of silicon abrasive mixed electrical discharge machining of tool steel. Mate Manuf Process 25:1041–1047
14. Kumar A, Maheshwari S, Sharma C, Beri N (2011) Analysis of machining characteristics in additive mixed electric discharge machining of nickel-based super alloy inconel 718. Mate Manuf Process 26:1011–1018
15. Kumar S, Singh R (2010) Investigating surface properties of OHNS die steel after electrical discharge machining with manganese powder mixed in the dielectric. Int J Adv Manuf Technol 50:625–633
16. Das A, Misra JP (2012) Experimental investigation on surface modification of aluminum by electric discharge coating process using TiC/Cu green compact tool-electrode. Mach Sci Technol Int J 16:601–623
17. Yan BY, Chen SL (1993) Effects of dielectric with suspended aluminum powder on EDM. J Chin Soc Mech Eng 14(3):307–312
18. Yan BY, Chen SL (1994) Characteristics of SKD11 by complex process of electric discharge machining using liquid suspended with aluminum powder. J Jpn Inst Light Metals 58(9):1067–1072
19. Yan BY, Chen MD (1994) Effect of ultrasonic vibration on electrical discharge machining characteristics of Ti–6Al–4V Alloy. J Jpn Inst Light Metals 44(5):281–285
20. Kansal HK, Singh S, Kumar P (2006) Performance parameters optimization (mulTi–characteristics) of powder mixed electric discharge machining (PMEDM) through Taguchi's method and utility concept. Indian J Eng Mater Sci 13:209–216
21. Abdulkareem S, Khan AA, Konneh M (2009) Reducing electrode wear ratio using cryogenic cooling during electrical discharge machining. Int J Adv Manuf Technol 45:1146–1151
22. Gill SS, Singh J (2010) Effect of Deep cryogenic treatment on machinability of titanium alloy (Ti–6246) in electric discharge drilling. Mate Manuf Process 25:378–385
23. Srivastava V, Pandey PM (2012) Effect of process parameters on the performances of EDM process with ultrasonic assisted cryogenically cooled electrode. J Manuf Process 3:393–402
24. Jafferson JM, Hariharan P (2013) Machining performance of cryogenically treated electrodes in microelectric discharge machining: a comparative experimental study. Mate Manuf Process 28:397–402
25. Bagchi TP (1993) Taguchi methods explained: practical steps to robust design. Prentice Hall of India Private Ltd, India, pp 11–19 **(0-87692-80804)**
26. Khan MAR, Rahman MM, Kadirgama K (2015) An experimental investigation on surface finish in die-sinking EDM of Ti–5Al–2.5Sn. Int J Adv Manuf Technol 77:1727–1740